IOP Publishing
Measurement Science and Technology
Meas. Sci. Technol. **31** (2020) 015204 (8pp)
https://doi.org/10.1088/1361-6501/ab33d3

A sensitive portable fluorometer coupled with miniaturized integrating sphere

Cheng-fu Chen[1,3], **John H Halford**[1] **and Dain M Harmon**[2]

[1] Department of Mechanical Engineering, University of Alaska Fairbanks, Fairbanks, AK 99775-5905, United States of America
[2] Department of Computer Science, University of Alaska Fairbanks, Fairbanks, AK 99775-5905, United States of America

E-mail: cchen4@alaska.edu

Received 27 February 2019, revised 15 July 2019
Accepted for publication 19 July 2019
Published 24 October 2019

Abstract

This paper presents a portable fluorescence detector with a tested limit of detection (LOD) at 0.4 nM of the fluorescein solution. This detector was prototyped with a miniaturized integrating sphere that couples a sample-filled glass flow-cell, a 450 nm laser diode, a 550 nm long-pass optical filter, and a light sensor. The integrating sphere is shown to improve the sensitivity and resolution of detection by collecting all the fluorescence emanation. A comparative study with two integrating spheres of 0.75-in. diameter, reflective versus black, shows that the former enables (1) a larger amount of irradiance at the light sensor, (2) a lower LOD, and (3) better resolution of detection. An estimation of the battery lifetime is given for various scenarios of operating this fluorometer for measurements.

Keywords: integrating sphere, portable fluorometer, fluorescence, detection

(Some figures may appear in colour only in the online journal)

Introduction

Fluorescence detection is a high-sensitivity technique that is able to determine analytes at very low concentrations down to the picomolar range. This technique is also selective, which is attributed to the excitation and emission spectra of the fluorophores in use. Its performance is generally determined by the spectral properties of fluorophores and its spectrometric match to the excitation light, as well as an appropriate arrangement of necessary optical components and the sensor with respect to the sample holder [1].

Instrumentation of the fluorescence detection technique is concerned with the resolution and lower limit of detection (LOD), operation time, and cost, as well as its portability if for field applications. Traditionally, a laser is used as a light source for its unique spectral features. It produces light that is monochromatic, which can excite fluorophores at a specific wavelength; collimated, which makes the flux focused in a direct path; and coherent, which provides an advantage more for information-processing techniques than the fluorescence detection. When combined with capillary electrophoresis (CE), laser-induced fluorescence (LIF) is a powerful analytical tool that has been routinely used to detect compounds of biological and environmental significance [2–4]. LIF has also been applied with microfluidic chips to implement various analytical techniques [5] and point-of-care testing [6]. To achieve good sensitivity, a photomultiplier tube (PMT) is commonly used in these applications to collect weak emission of fluorescence from the fluorophore. An integrated CE-LIF on a microchip for the detection of various fluorophore compounds has been demonstrated with a decent LOD at the nanomolar or more diluted scale. Examples of such work include the detection of fluorescein solutions with a LOD at 50 nM [5] or 1.1 pM [7], and the dye DY636-COOH in water with a LOD at 26 nM [6].

Compared to the traditional laser, semiconductor-based light emitting diodes (LEDs) and laser diodes (LDs) are relatively compact and cheap, enabling low-cost and portable detection devices for field applications. Flaschka *et al* [8] pioneered implementing a LED-integrated detection technique with a phototransistor in the 1970s. Since then, various light source colors and advanced photo detectors have

[3] Author to whom any correspondence should be addressed.

been implemented for LED-induced fluorescence detection (LED-IFD) [9–13]. An ultraviolet (UV) LED-IFD technique emerged in 2002, when UV LEDs became commercially available; the light in the UV or deep blue spectral range enables a wider range of selection for the excitation spectrum. This allowed researchers to develop new UV-excited fluorescence techniques for detecting molecules or chemical compounds that are environmentally and biologically important [14]. Examples include the detection of aerosol particles [15, 16] and pharmaceutically active products in aquatic environments [17].

Compared to LEDs, the light from laser diodes is more spectrally centered, with a full-width half-max (FWHM) about ten times narrower. The LD-induced fluorescence detection (LD-IFD) has been implemented in a wide spectral range. Examples include the use of a laser diode peaked at 670 nm [18] and of a UV LED [19] for detecting chlorophyll; a pulsed laser diode emitting at 630 nm for DNA sequencing in capillary gel electrophoresis [20]; a confocal red diode laser at 635 nm integrated with a PMT and microfluidic CE to detect Cy-5 labelled antibodies [21]; and blue LDs emitting in 397–450 nm for detecting amino acids [18, 22], nitrogen dioxide and iodine monoxide [23] (the detection of which was enhanced with a cavity), and stained DNA [24], and exciting the chlorophyll fluorescence for assessing disease [25].

However, because the semiconductor-based LEDs and LDs have a relatively lesser spectral radiance in wavelength than traditional lasers, they impose an additional design consideration of retaining an acceptable efficiency of excitation while reducing scattering/refraction/reflection of light [26]. This is the key to successful instrumentation of a sensitive LED-IFD or LD-IFD technique.

Most fluorescence detectors are implemented in the sense that the photo detector (light sensor) receives only a fraction of the fluorescence emission emanated from the sample. With the same hardware setting, the sensitivity of detection could be further improved, should all the emanated fluorescence be collected from the 4π steradians for detection. Such an improvement, once made, would facilitate the development of a portable fluorescence detection technique with an acceptable detection sensitivity.

The idea of collecting all the emanated fluorescence is realized in integrating-sphere-based radiometry, in which a reflective sphere of diameter 12 in. or larger is used to quantify the spectral properties of a light source [27], absorbance of samples [28], or the photoluminescence quantum yield of phosphors [29]. In theory, the continuous reflection of fluorescence emission on the sphere wall increases the irradiance received by the light sensor by a factor of $\rho/(1-\rho)$ [30], where ρ is the reflectivity of the wall. The idea that a very large gain can be acquired in the limit of a perfect reflection inspires a potential application of the integrating sphere to sensitive fluorescence detection. For example, a 66-fold signal increase in detection has been demonstrated with an ellipsoidal reflection mirror [31]. This idea was also recently demonstrated using a miniaturized reflective cavity, e.g. LED-IFD implemented within an 1-in. dome-shaped reflector [32] and a 1 cm-radius hemispherical reflector with $\rho > 0.9$ [33], and detection of urobilin concentrations down to 0.5 pM within a silica-fused 2-in.-diameter column [34]. These demonstrations open an avenue to the use of a miniaturized integrating sphere for portable fluorescence detection with good sensitivity of detection.

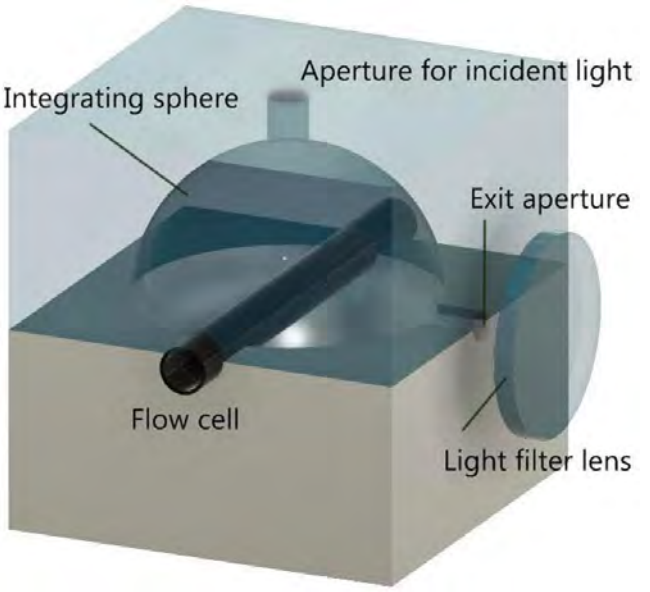

Figure 1. Schematic of the fluorescence detector coupled with an integrating sphere.

This paper presents a portable fluorometer coupled with an integrating sphere of ¾-in. diameter with a demonstrated LOD of fluorescein concentration at 0.4 nM.

Materials and method

Figure 1 is a schematic of the fluorescence detector design, the top portion of which is transparently painted to show its interior arrangement. This design features a spherical cavity as the light reflection and collection chamber. The cavity has a polished wall for reflecting light, and is referred to as the integrating sphere herein. A glass flow cell is placed across the integrating sphere. The excitation light enters the cavity from an aperture opened at the north pole of the integrating sphere, and is focused on the flow cell to excite fluorescence emission from the sample solution. Both the excitation light and fluorescence emission co-exist and reflect within the cavity. The excitation light in part hits the analyte and in part bounces back and forth to continue to excite the analyte. For measurement, an optical filter lens is placed between the exit aperture and the light sensor. The exit aperture is at an azimuth of 90° from the light source. Because reflected transmission of the excitation light has less spectral radiance than the direct transmission when reaching the detection port, the arrangement of ports in a 90-degree configuration can reduce the noise due to excitation. No baffle is used in this design. In such an arrangement, both the co-existing excitation light and fluorescence will be apparent at the exit aperture. An optical filter lens is used to pick up the fluorescence for detection by a light sensor (not shown).

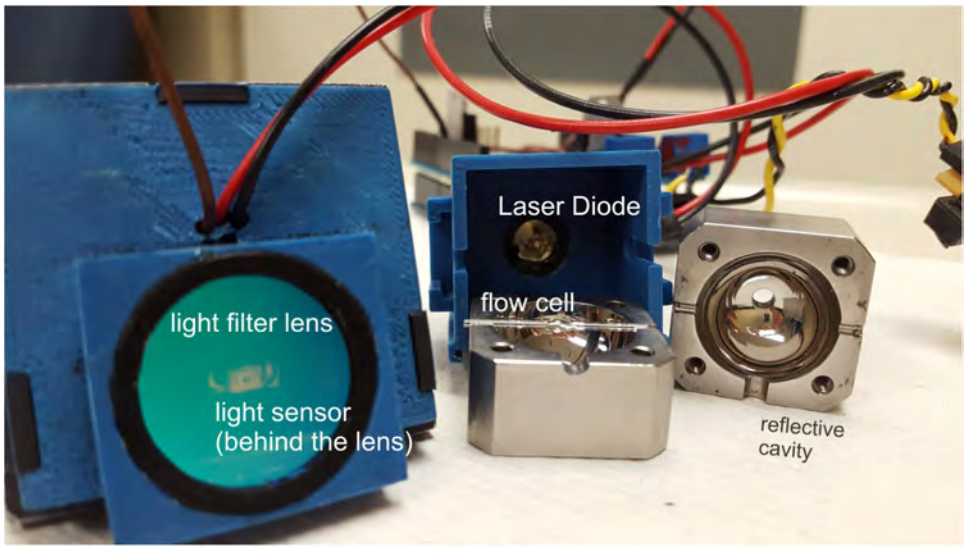

Figure 2. Exploded view of the detection unit. Reproduced with permission from [37]. Copyright © 2018, IEEE.

Figure 2 shows an exploded view of the prototype. A housing was 3D printed to tightly assemble the integrating sphere with a laser diode (as the light source). A few trials were conducted to ensure that the laser diode is aligned to focus on the flow cell. Another housing, which assembles the light filter lens and the light sensor, was also 3D-printed for easy and rigid assembly with the first housing. Each of the components is described below.

Two integrating spheres, reflective versus black, were prototyped individually for a comparative study. For portability, both integrating spheres were made as a spherical cavity in a 1-in. cube. The first integrating sphere was made using a 403 stainless steel cube, 1 in. long on each side, as shown in figure 3. This cube was first cut in half, and then ball-milled to make a hemispherical cavity, 0.75-in. in diameter. The milled radius was measured with a micrometer screw gauge and exhibited a value in the range 0.375 ± 0.003 in. The milled surface was polished with an ammonia-based polish cream (Metal Polish Cream or Blue Magic) to remove the surface oxides for better reflectivity. A polished cavity is shown in figure 3. The second integrating sphere was 3D-printed with black acrylonitrile butadiene styrene (ABS), which is relatively rough as compared to the steel sphere.

Our experience suggests that maximizing the exposed volume of analyte improves the sensitivity of detection. Therefore, at the middle of the flow cell shown in figure 3 is a bulge (aka bubble cell [35, 36]) where the excitation light exposes the sample solution. The bubble cell was made out of a glass tube of 0.05 in. ID and 0.06 in. OD by a skilled glass smith. The flow cell is placed across the integrating sphere through the grooves cut at two sides of the stainless steel block. Each end of the flow cell was press-fit to the Tygon tubing, which allows for a tight assembly with the integrating sphere by tightening four screws at each corner of the stainless steel blocks. Once assembled, a spherical cavity is formed with four ports, two for holding the flow cell and the others are apertures for the light inlet and outlet.

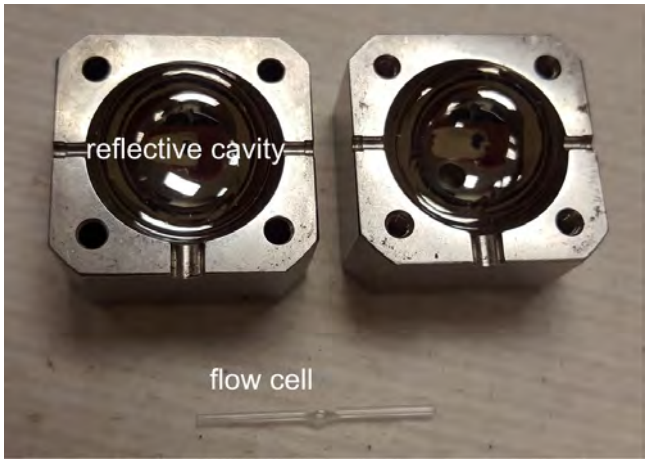

Figure 3. The integrating sphere and flow cell. The (narrower) grooves on the left and right sides of each block are cut for holding the flow cell. Once assembled, the (wider) grooves at the bottom of each block form an aperture for the light source to irradiate the analyte solution in the flow cell. Reproduced with permission from [37]. Copyright © 2018, IEEE.

As sold, the laser diode produces a collimated spot (with a collimating lens), which is set to just cover the bubble cell with a negative focal length in our assembly. The negative focal length is fixed in our design through the assembly of 3D printed housing for the laser diode and the integrating sphere. Although such a focusing scheme reduces the radiant flux density of the excitation light at the flow cell, it allows for a gain in the exposure area of the flow cell to the excitation light.

The repeatability of the focusing procedure is ensured by an asymmetric mounting scheme implemented in our revised design. An asymmetric mounting mechanism was 3D printed, with the male design placed in the housing of the laser diode and female design in that of the integrating sphere. The asymmetry was carefully configured so that the collimated spot (which is rectangular-like) aligns in the longitudinal direction of the flow cell.

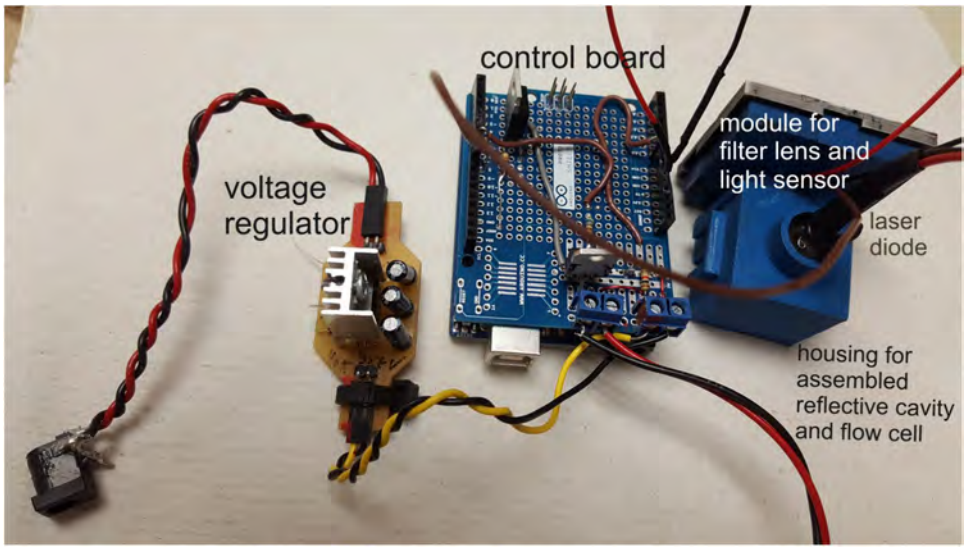

Figure 4. The integrating sphere-coupled laser diode-induced fluorescence detection system. Reproduced with permission from [37]. Copyright © 2018, IEEE.

Fluorescein was used for evaluating the portable detection instrumentation. Fluorescein absorbs and emits at 493 nm and 513 nm, respectively. A blue laser diode (Osram Opto Semiconductors GmbH) with a lasing wavelength peak at 450 nm with a FWHM spectral width 2 nm was selected for its low power consumption and low cost. This blue laser diode consumes 0.53W to generate a 80 mW radiant flux.

Because the excitation light and fluorescence co-exist in the integrating sphere, for detection a long-pass filter with a cut-on wavelength at 550 nm was used to selectively pick up fluorescence for detection.

A color sensor, which consumes 0.25mW, was used as the light detector. The responsivity of this color sensor is in the wavelength range of 300 nm–1100 nm of light, with the maximum at 700 nm. Its responsivity in the range of our interest, 450 nm–600 nm, is about 60 %–90% of the maximum value, and exhibits a linear relation to the wavelength of the light. The light sensor reacts on an irradiance linearly in the range of [0.001, 100] μW cm^{-2}.

Fluorescein solutions were prepared by starting from a concentration of 1 mM of fluorescein in 0.5 l Milli-Q down to 100 nM by a dilution factor of 0.1, and then fractionally down to various concentrations, sequentially.

Results

Figure 4 shows the functional detector for testing, in which the assembled detection unit (the housing that contains the laser diode, integrating sphere, flow cell, filter lens, and light sensor) has a footprint less than 1.5 in. $\times$ 1.5 in. The detection unit is directed through an Arduino board, which controls an N-channel MOSFET on demand to turn on/off the laser diode for excitation. A linear 3.3 V voltage regulator was used to modulate the voltage for the laser diode. Readings from the light sensor were processed through the Arduino board to a laptop for recording the results, but can also be transmitted via Bluetooth to Android-based smart phones.

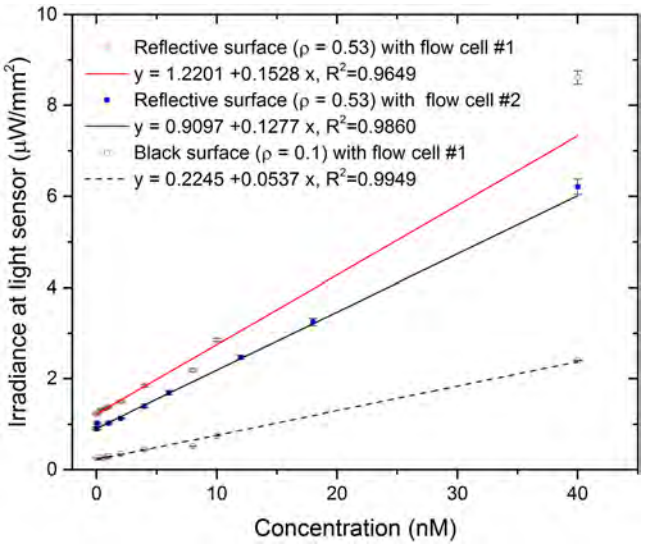

Figure 5. Comparison of integrating sphere surface reflectivity for measured irradiance of fluorescence emitted from fluorescein solution at various concentrations.

The lower bound of the battery lifetime can be estimated by a bulk number of the total power consumption of the fluorometer system, which is capped by 5 V at the current limit 500 mA, or 2.5 W, as constrained by the Arduino board. The fluorometer system can be operated with a standard 550 milliAmp hour (mAh) 9 V battery, which stores an equivalent energy of 4.95 W h. Given that the total power consumption of the fluorometer system is capped by 2.5 W as constrained by the Arduino board, and assuming that the system operates continuously, the lifetime is estimated at 1.98 h.

In practice, our fluorometer is designed for power savings. Because the laser diode is more power-hungry than all other electronic components in the fluorometer system, our design considers activating the laser diode on demand. When connected to a battery, the system automatically stands by, during which 61 mA is continuously drawn from the battery. The laser diode is activated for 0.6 second at each demand, during which

Table 1. Averaged irradiance measured with its 3σ value (with flow cell #1).

Concentration of fluorescein (nM) x	Measured irradiance (μW mm^{-2})				Irradiance ratio y^R/y^B
	Reflective integrating sphere		Black integrating sphere		
	$y^R \pm 3\sigma$	S/N	$y^B \pm 3\sigma$	S/N	
0 (blank)	1.2277 ± 0.0121	—	0.2583 ± 0.0054	—	4.8
0.4	1.3105 ± 0.0108	5.2	0.2607 ± 0.0042	0.4	5.0
0.8	1.3487 ± 0.0153	6.3	0.2783 ± 0.0069	2.3	4.8
1	1.3781 ± 0.0132	8.5	0.2974 ± 0.0057	4.9	4.6
2	1.4893 ± 0.0183	12.0	0.3446 ± 0.0026	14.4	4.3
4	1.8404 ± 0.0238	23.0	0.4439 ± 0.0077	19.7	4.1
8	2.1846 ± 0.0254	34.0	0.5182 ± 0.0088	25.2	4.2
10	2.8504 ± 0.0348	44.1	0.7428 ± 0.0109	39.7	3.8
40	8.6130 ± 0.1473	50.0	2.3988 ± 0.0378	56.1	3.6

an additional 44 mA is drawn from the battery, and then the system stands by again. (The duration of 0.6 s is an adjustable parameter, to accommodate the light sensor for collecting the measurement data.) When activated, the laser diode consumes 44 mA $\times \frac{0.6\,\text{s}}{3600\,\text{s}}$ per hour, or 0.0073 mA per hour. If the laser diode is fired up f times per hour, it will consume $0.0073f$ mA per hour. Together with the consumption in standby of 61 mA per hour, the system consumes $61 + 0.0073f$ mA per hour in the combined standby/activation modes. Therefore, the battery lifetime can be estimated as $550/(61 + 0.0073f)$ hours. This parametric expression estimates the battery lifetime for various application scenarios. For example, if 600 readings are made per hour ($f = 600$), the lifetime would be 8.41 h. At most the device can take up to 6000 readings per hour when the laser diode is continuously activated (i.e. the laser is activated 100 times per minute, or $f = 6000$). In this condition, the battery lifetime would be 5.24 h, during which the fluorometer would take up to 31440 readings.

These estimates are maximum values; practical battery lifetimes are shorter and are dependent on the quality of the batteries in use.

Figure 5 compares the irradiance received at the light sensor with the reflective and black integrating spheres. Figure 5 also compares the detection with two different glass flow cells. Each data point is the average of 25 repeated measurements of the same fluorescein solution, with the error bars for three standard deviations (3σ). Data plotted in figure 5 is presented in table 1 using flow cell #1.

Discussion

Limit and resolution of detection

LOD is the lowest concentration at which the fluorescence signal dominates the noise in a measurement. LOD can be determined by calculating the signal-to-noise ratio of each measured irradiance, as discussed below.

In our design, because the fluorescence emission co-exists with the beam of excitation in the integrating sphere, the irradiance picked up by the light sensor is essentially composed of (1) the irradiance of fluorescence emission from the analyte, which is the signal to be determined, and (2) the filtered spectral irradiance from other sources, which is the detected background signal. The background signal is mainly attributed to the spectral irradiance of the excitation light 'leaking' through the optical filter. Ramon scattering, if any, will also be part of the background signal. The background signal can be determined by the irradiance measured at the zero concentration, which is referred to as the 'blank' response of the instrumented fluorescence detector indicated in table 1.

Table 2. Information for calculating the theoretical LOD.

	Reflective integrating sphere	Non-reflective integrating sphere
Linear-fit equation (μW mm^{-2})	$y = 1.220 + 0.1528\,x$	$y = 0.2245 + 0.0537\,x$
$y_{\text{blank}} + 3\sigma_{\text{blank}}$ (μW mm^{-2})	$1.2277 + 0.0121$	$0.2583 + 0.0054$
Theoretical LOD (nM)	0.13	0.73
Measured LOD (nM)	0.4	0.8

The signal (S) can thus be calculated by subtracting the blank reading from each sample reading (y, e.g. y^R or y^B in table 1) as

$$S = y - y_{\text{blank}} \tag{1}$$

where y_{blank} is the blank response of the fluorescence detector. The blank reading and the sample reading were collected under the same measurement conditions at the authors' best practice.

The noise is estimated by the square root of the square sum of the three standard deviations of the measured data at a concentration (3σ) and of the blank reading ($3\sigma_{\text{blank}}$):

$$N = \sqrt{(3\sigma)^2 + (3\sigma_{\text{blank}})^2}. \tag{2}$$

The S/N ratio is calculated accordingly. The measured LOD is then determined by the lowest measured concentration at which the S/N ratio is greater than 1. From the results summarized in table 1, it can be seen that the integrating sphere with a reflective surface has a LOD at 0.4 nM, and a LOD at 0.8 nM for the black sphere.

The theoretical LOD is calculated as the x-intercept of the linearly-fitted curves (figure 5) at the y value equal to $y_{\text{blank}} + 3\sigma_{\text{blank}}$. Table 2 summarizes the numbers for the calculations. For the fluorescence detector coupled with the reflective sphere, the calculated LOD is 0.13 nM, as opposed to its measured value of 0.4 nM. Recall that the signal-to-noise ratio at 0.4 nM is 5.2, implying that this prototyped detector has room to experimentally explore its lowest possible LOD. For detection with the black sphere, the LOD has a theoretical value of 0.73 nM, which is very close to its measured value 0.8 nM.

The resolution of detection can be indicated by the slope of each linearly fitted curve in figure 5. The steeper slope associated with the steel integrating sphere indicates a better resolution in detection.

Enhancement of fluorescence detection in reflective integrating sphere

Two sets of fluorescence detection are compared to illustrate the enhancement of detection by the reflective integrating sphere. One set was measured by an integrating sphere made of stainless steel that has a reflectivity $\rho = 0.53$ at 450 nm [38], and the other set by a 3D-printed sphere with a black ABS material that has a relatively rough non-reflective interior surface. ABS is a common 3D printing material with a reflectivity of about 0.1 [39].

In theory, the integrating sphere can increase the irradiance by a factor of $\rho/(1-\rho)$ [30], where ρ is the reflectivity of the sphere wall. For the reflective sphere made of stainless steel with $\rho = 0.53$, the theoretical gain is 1.1, about ten times more than that of the black cavity. Experimentally, based on the ratio of the measured irradiance listed in the last column of table 1, the reflective integrating sphere can provide a gain in the detected irradiance of about 4 to 5 times.

Both the experimental and theoretical results conclude that an integrating sphere of similar shape, with a reflective surface capable of collecting light in the 4π steradians, can offer a gain in the detected fluorescence [31–33]. The gain can be even more significant when the reflectivity is closer to 1, which can be realized with a well-polished aluminium surface, a gold-deposited surface, or a processed surface made by fumed silica powder [34].

The size of the integrating sphere can affect the measured irradiance in a few aspects. First, the theoretical gain in irradiance can be formulated as $\rho/(1-\rho(1-f))$, where f is the port fraction of the integrating sphere [40]. In our design, there are four ports, two for placing the flow cell, one as the aperture for the excitation light, and one as the exit aperture of light for detection. The total areas of the four ports typically are a constant number. The port fraction, a ratio of the port areas to the total wall surface of the integrating sphere, is smaller for a larger sphere. Therefore, a larger sphere contributes to a larger gain. A larger integrating sphere also facilitates the use of a baffle for mechanically diverting or reflecting the light inside the sphere, which in some conditions would further improve the sensitivity of detection. (Baffles were not considered in our design reported herein.) However, a smaller integrating sphere is advantageous due to its portability. A trade-off in selecting the size of the integrating sphere must be considered for sensitivity and portability. In this work, a spherical cavity of 0.75-in. diameter was demonstrated for both an acceptable performance of detection and portability.

The role of flow cell in detection

The glass flow cell can trap light—like an optical guide. Because glasses have a larger index of refraction than air, some portion of the light will be trapped within the glass flow cell and propagate longitudinally to the ports of the flow cell. Any fluorescence trapped in the flow cell can be counted as leaking, meaning not received by the light sensor. Quantifying the leaking fluorescence is beyond the scope of this paper, but can be addressed by placing the light sensor at one port of the flow cell (with some modified work on the housing and adaptors), to measure the leaking fluorescence, if detectable.

The bubble cell is the bulged portion made in the glass flow cell where the excitation light exposes the analyte-laden solution. The shape and size of the bubble cell influences light transmission and refraction, and, in turn, the fluorescence emission and the result of detection. In our design the bubble cell should be ideally spherical, but the customer-made cell was oval-like and not uniform from one to another. We surmise that such non-uniformity leads to a flow-cell-dependent detection result. In figure 5 the instrumental responses with two different flow cells (#1 versus #2) are compared. The results with flow cell #1 are listed in table 1. Flow cell #2 results indicate a LOD at 0.2 nM (S/N = 1.1) with a rougher resolution, as told by the gradual slope of the fitted line versus the steep slope associated with flow cell #1 in figure 5. We also conducted detection with another flow cell (#3) and obtained a LOD at 0.16 nM but with S/N 3.2. We would expect a trend of decreasing LODs in a decreasing S/N number, but this was not observed from these results with the three flow cells used. We conclude that the inconsistent shape and size of the bubble cell has significant influence on the determination of resolution (the slope of the fitted curve) and LOD (the y-interception of the fitted curve).

Influence of Raman scattering from water

Given the excitation photons at an energy of wavelength 450 nm and the Raman shift of water in 3000–3700 cm^{-1} [41], the photons of Stokes scattering from the H_2O molecules have a wavelength in the range 520–540 nm, as can be calculated per the Raman shift equation. Although we adopted a 550 nm long-pass optical filter and determined the signal by subtracting the reading for the solvent (water) only from that of the sample solution, per equation (1), a trace amount of detected response would probably be attributed to Raman scattering. The influence of Raman scattering on detection can be addressed by shifting the peak wavelength of Raman scattering away from the wavelength range of detection. It can possibly be achieved by using an excitation light of shorter

peak wavelength, or an optical filter of spectral range away from the wavelength of Raman scattering.

Modular design for easy interchange and replacement of components

The laser diode is compress-fitted in a 3D printed housing, which allows for quickly switching one laser diode module to another of the same housing diameter (12 mm). For field deployment, the housing unit would be additionally screwed or fastened. Each laser diode module must be equipped with its own voltage regulator and power board, making it ready for plug-and-play.

Replacing the optical filter needs a few more steps, as it is sandwiched between the integrating sphere and the light sensor. The housing of the light sensor is engaged to that of the optical filter by the groove assembly, as is the housing of the optical filter to that of the integrating sphere. To interchange the optical filter, one first disengages (by manually sliding) the housings of the light sensor from that of the optical filter, and in turn from that of the integrating sphere. On the other end, the housing of the optical filter adopts the snap-fit joint design for assembly. To swap the assembled optical filter with another of the same diameter (1 in.), simply press each joint to dissemble the housing.

The driver (controller) has been programmed to work with an excitation light in the light sensor's responsivity $> 50\%$ in the wavelength range of 400 nm–900 nm. Therefore, any interchange of the laser diode and/or optical filter in the mentioned spectral range, once assembled, requires no additional work and the fluorometer device is readily functional.

Conclusions

In this paper an integrating-sphere-coupled, portable fluorescence detector was presented with the design, prototyping, and testing results. The measured LOD for measuring the fluorescein solution is 0.4 nM with a signal-to-noise ratio larger than 5. Such a sensitivity of detection is attributed to the use of an integrating sphere for a higher gain in the collected irradiance for detection. The effectiveness of using the miniaturized integrating sphere for improving the LOD was herein demonstrated and explained, both experimentally and theoretically. For this prototyped fluorometer presented, its lower LOD could be further explored with the fluorescein solutions and other types of fluorophore in the future. For portability, this paper also provides an estimation of the battery lifetime.

Acknowledgment

The authors thank Mr Joe Michalski for ball-milling the integrating sphere and Mrs. Joan Welc-LePain for proof reading the manuscript. This material is based in part upon work supported by the National Aeronautics and Space Administration (NASA) under Grant No. NNNX15AM63A. This document contains trade secrets or otherwise proprietary confidential information owned by the University of Alaska Fairbanks.

ORCID iDs

Cheng-fu Chen https://orcid.org/0000-0001-7183-1918

References

[1] Resch-Genger U *et al* 2005 How to improve quality assurance in fluorometry: fluorescence-inherent sources of error and suited fluorescence standards *J. Fluorescence* **15** 337–62
[2] Páez X and Hemández L 2001 Biomedical applications of capillary electrophoresis with laser-induced fluorescence detection *Biopharm. Drug Dispos.* **22** 273–89
[3] Lada M W, Vickroy T W and Kennedy R T 1997 High temporal resolution monitoring of glutamate and aspartate *in vivo* using microdialysis on-line with capillary electrophoresis with laser-induced fluorescence detection *Anal. Chem.* **69** 4560–5
[4] Meagher R J, Hatch A V, Renzi R F and Singh A K 2008 An integrated microfluidic platform for sensitive and rapid detection of biological toxins *Lab Chip* **8** 2046–53
[5] Li H F, Lin J M, Su R G, Uchiyama K and Hobo T 2004 A compactly integrated laser-induced fluorescence detector for microchip electrophoresis *Electrophoresis* **25** 1907–15
[6] Berner M, Hilbig U, Schubert M B and Gauglitz G 2017 Laser-induced fluorescence detection platform for point-of-care testing *Meas. Sci. Technol.* **28** 085701
[7] Fu J-L, Fang Q, Zhang T, Jin X-H and Fang Z-L 2006 Laser-induced fluorescence detection system for microfluidic chips based on an orthogonal optical arrangement *Anal. Chem.* **78** 3827–34
[8] Flaschka H, McKeithan C and Barnes R 1973 Light emitting diodes and phototransistors in photometric modules *Anal. Lett.* **6** 585–94
[9] Anfalt T, Graneli A and Strandberg M 1976 Probe photometer based on optoelectronic components for the determination of total alkalinity in seawater *Anal. Chem.* **48** 357–60
[10] Wolfbeis O S, Schaffar B P H and Kaschnitz E 1986 Optical fibre titrations. Part 3. Construction and performance of a fluorimetric acid-base titrator with a blue LED as a light source *Analyst* **111** 1331–4
[11] Liu M S and Amirkhanian V D 2003 DNA fragment analysis by an affordable multiple-channel capillary electrophoresis system *Electrophoresis* **24** 93–5
[12] Su A-K and Lin C-H 2003 Determination of riboflavin in urine by capillary electrophoresis-blue light emitting diode-induced fluorescence detection combined with a stacking technique *J. Chromatogr.* B **785** 39–46
[13] Chabinyc M L *et al* 2001 An integrated fluorescence detection system in poly(dimethylsiloxane) for microfluidic applications *Anal. Chem.* **73** 4491–8
[14] Hapuarachchi S, Janaway G A and Aspinwall C A 2006 Capillary electrophoresis with a UV light-emitting diode source for chemical monitoring of native and derivatized fluorescent compounds *Electrophoresis* **27** 4052–9
[15] Cabalo J, DeLucia M, Goad A, Lacis J, Narayanan F and Sickenberger D 2008 Overview of the TAC-BIO detector *Proc. SPIE* **7116** 71160D
[16] Davitt K *et al* 2005 290 and 340 nm UV LED arrays for fluorescence detection from single airborne particles *Opt. Express* **13** 9548–55
[17] Patrolecco L, Ademollo N, Grenni P, Tolomei A, Barra Caracciolo A and Capri S 2013 Simultaneous determination of human pharmaceuticals in water samples by solid phase extraction and HPLC with UV-fluorescence detection *Microchem. J.* **107** 165–71
[18] Higashijima T, Fuchigami T, Imasaka T and Ishibashi N 1992 Determination of amino acids by capillary zone

electrophoresis based on semiconductor laser fluorescence detection *Anal. Chem.* **64** 711–4
[19] Buah-Bassuah P K, von Bergmann H M, Tatchie E T and Steenkamp C M 2008 A portable fibre-probe ultraviolet light emitting diode (LED)-induced fluorescence detection system *Meas. Sci. Technol.* **19** 025601
[20] Lieberwirth U *et al* 1998 Multiplex dye DNA sequencing in capillary gel electrophoresis by diode laser-based time-resolved fluorescence detection *Anal. Chem.* **70** 4771–9
[21] Jiang G, Attiya S, Ocvirk G, Lee W E and Harrison D J 2000 Red diode laser induced fluorescence detection with a confocal microscope on a microchip for capillary electrophoresis *Biosens. Bioelectron.* **14** 861–9
[22] Melanson J E and Lucy C A 2000 Violet (405 nm) diode laser for laser induced fluorescence detection in capillary electrophoresis *Analyst* **125** 1049–52
[23] Kasyutich V L, Bale C S E, Canosa-Mas C E, Pfrang C, Vaughan S and Wayne R P 2003 Cavity-enhanced absorption: detection of nitrogen dioxide and iodine monoxide using a violet laser diode *Appl. Phys.* B **76** 691–7
[24] Shapiro H M and Perlmutter N G 2001 Violet laser diodes as light sources for cytometry *Cytometry* **44** 133–6
[25] Anderson B, Eghan M J, Asare-Bediako E and Buah-Bassuah P K 2012 Violet diode laser-induced chlorophyll fluorescence: a tool for assessing mosaic disease severity in cassava (Manihot esculenta Crantz) cultivars *Environ. Technol.* **33** 367–72
[26] Novak L, Neuzil P, Pipper J, Zhang Y and Lee S 2007 An integrated fluorescence detection system for lab-on-a-chip applications *Lab Chip* **7** 27–9
[27] Hanselaer P, Keppens A, Forment S, Ryckaert W R and Deconinck G 2009 A new integrating sphere design for spectral radiant flux determination of light-emitting diodes *Meas. Sci. Technol.* **20** 095111
[28] Gaigalas A K, He H-J and Wang L 2009 Measurement of absorption and scattering with an integrating sphere detector: application to microalgae *J. Res. Natl Inst. Stand. Technol.* **114** 69–81
[29] Gorrotxategi P, Consonni M and Gasse A 2015 Optical efficiency characterization of LED phosphors using a double integrating sphere system *J. Solid State Light.* **2** 1
[30] Finkel M W 1970 Integrating sphere theory *Opt. Commun.* **2** 25–28
[31] Yao M and Wolfe J C 2007 A laser-induced fluorescence biosensor by using ellipsoidal reflector *Opt. Laser Technol.* **39** 1040–5
[32] Park B, Kwon K and Yu K 2012 Non-imaging fluorescence detection system with hemispherical dome reflectors *Int. Conf. on Optical MEMS and Nanophotonics* pp 196–7
[33] Kwon K, Park B, Shim J and Yu K 2012 Fluorescence detection system with miniaturized integrating sphere *Int. Conf. on Optical MEMS and Nanophotonics* pp 235–6
[34] Bixler J N *et al* 2014 Ultrasensitive detection of waste products in water using fluorescence emission cavity-enhanced spectroscopy *Proc. Natl Acad. Sci.* **111** 7208–11
[35] Rodat A, Gavard P and Couderc F 2009 Improving detection in capillary electrophoresis with laser induced fluorescence via a bubble cell capillary and laser power adjustment *Biomed. Chromatog.* **23** 42–7
[36] Soper S A and Legendre B L 1998 Single-molecule detection in the near-IR using continuous-wave diode laser excitation with an avalanche photon detector *Appl. Spectrosc.* **52** 1–6
[37] Harmon D M, Chen C-F and Halford J H 2018 Portable fluorescence detection platform with integrating sphere *2018 40th Annual Int. Conf. of the IEEE Engineering in Medicine and Biology Society* (IEEE) pp 2889–92
[38] Zwinkels J C, Noël M and Dodd C X 1994 Procedures and standards for accurate spectrophotometric measurements of specular reflectance *Applied Optics* **33** 7933–44
[39] Morgan R V, Reid R S, Baker A M, Lucero B and Bernardin J D 2017 Emissivity measurements of additively manufactured materials *Los Alamos National Laboratory Technical Report* LA-UR-17-20513
[40] Labsphere 2017 Integrating Sphere Theory and Applications www.labsphere.com/site/assets/files/2551/integrating_sphere_theory_apps_tech_guide.pdf (Accessed: 16 October 2019)
[41] Lawaetz A J and Stedmon C A 2009 Fluorescence intensity calibration using the Raman scatter peak of water *Appl. Spectrosc.* **63** 936–40